Improved shell model of turbulence

Victor S. L'vov,[1] Evgenii Podivilov,[1,2] Anna Pomyalov,[1] Itamar Procaccia,[1] and Damien Vandembroucq[1]
[1]*Department of Chemical Physics, The Weizmann Institute of Science, Rehovot 76100, Israel*
[2]*Institute of Automatization, Siberian Branch of the Russian Academy of Science, Novosibirsk 630090, Russia*
(Received 16 March 1998)

We introduce a shell model of turbulence that exhibits improved properties in comparison to the standard (and very popular) Gledzer, Ohkitani, and Yamada (GOY) model. The nonlinear coupling is chosen to minimize correlations between different shells. In particular, the second-order correlation function is diagonal in the shell index and the third-order correlation exists only between three consecutive shells. Spurious oscillations in the scaling regime, which are an annoying feature of the GOY model, are eliminated by our choice of nonlinear coupling. We demonstrate that the model exhibits multiscaling similar to the GOY model. The scaling exponents are shown to be independent of the viscous mechanism as is expected for Navier-Stokes turbulence and other shell models. These properties of the model make it optimal for further attempts to achieve understanding of multiscaling in nonlinear dynamics. [S1063-651X(98)10007-7]

PACS number(s): 47.27.−i

I. INTRODUCTION

Shell models of turbulence [1–5] are simplified caricatures of the equations of fluid mechanics in wave-vector representation; typically they exhibit anomalous scaling even though their nonlinear interactions are local in wave-number space. Their main advantage is that they can be studied via fast and accurate numerical simulations, in which the values of the scaling exponents can be determined very precisely. Our interest in shell models stemmed from our efforts to develop analytic methods for the calculation of the numerical values of the scaling exponents [6]. In trying to do so we discovered that the most popular shell model that was treated in the literature, the so-called Gledzer, Ohkitani, and Yamada (GOY) model [1,2], poses very tedious calculations because it exhibits slowly decaying correlations between velocity components with different wave numbers. In addition, it has large oscillations around the power-law behavior in the scaling regime, making the numerical calculation of the scaling exponents less obvious than advertised. We therefore derived a model that exhibits similar anomalies of the scaling exponents but much simpler correlation properties, and much better scaling behavior in the inertial range. Since there is a significant number of researchers who are interested in this type of model independent of the analytic calculability of the exponents, we decided to present the model *per se*, discuss its good properties, display the results of numerical simulations, and compare it to the standard Gledzer, Ohkitani, and Yamada model. These are the aims of this paper.

In Sec. II we review the popular GOY model, and explain the shortcomings that induced us to consider a different model. Section III introduces the model, which we propose to call the Sabra model; we discuss the phase symmetries and correlations, stressing the much improved properties. Section IV discusses numerical simulations from the algorithmic point of view. Section V contains the results of numerical simulations and fit procedures for accurate calculations of the scaling exponents. We believe that this section contains methods that should be used in the context of any shell model, and go beyond naive log-log plots. Section IV presents a discussion of the limitations in computing high-order exponents. We demonstrate that beyond ζ_8 one needs exponentially long running times to extract reliable exponents. The evaluation of ζ_{10} requires about one million turnover times of the largest scales. We believe that similar limitations are important also in other examples of multiscaling, including Navier-Stokes turbulence. Section VII demonstrates the universality of the scaling exponents with respect to the viscous mechanism, and Sec. VIII offers a short summary.

II. REVIEW OF THE GOY MODEL

A. Basic properties

In the past, considerable attention has been given to one particular version of shell models, the so-called GOY model [1,2]. This model describes the dynamics of a complex ''Fourier'' component of a scalar velocity field that is denoted as u_n. The associated wave number is one-dimensional, denoted as k_n. The index n is discrete, and is referred to as the ''shell index.'' The equations of motion read

$$\frac{du_n}{dt} = i(ak_{n+1}u_{n+2}u_{n+1} + bk_n u_{n+1}u_{n-1} + ck_{n-1}u_{n-1}u_{n-2})^* - \nu k_n^2 u_n + f_n, \tag{1}$$

where the asterisk stands for complex conjugation. The wave numbers k_n are chosen as a geometric progression

$$k_n = k_0 \lambda^n, \tag{2}$$

with λ being the ''shell spacing'' parameter. f_n is a forcing term that is restricted to the first shells. The parameter ν is the ''viscosity.'' In the limit of zero viscosity, one can arrange the model to have two quadratic invariants. Requiring that the energy

$$E=\sum_n |u_n|^2 \tag{3}$$

will be conserved leads to the following relation between the coefficients a, b, and c:

$$a+b+c=0. \tag{4}$$

A second quadratic quantity that is conserved is then

$$H=\sum_n (a/c)^n |u_n|^2. \tag{5}$$

Although nonpositive, this second invariant is often associated with ''helicity.''

The main attraction of this model is that it displays multiscaling in the sense that moments of the velocity depend on k_n as power laws with nontrivial exponents:

$$\langle |u_n|^q \rangle \propto k_n^{-\zeta_q}, \tag{6}$$

where the scaling exponents ζ_q exhibit nonlinear dependence on q. We expect such scaling laws to appear in the ''inertial range'' with shell index n much larger than the largest shell index that is effected by the forcing, denoted as n_L, and much smaller than the shell indices affected by the viscosity, the smallest of which will be denoted as n_d.

We will refer to the moments as ''structure functions.'' For even $q=2m$ we use the usual definition:

$$S_{2m}(k_n)=\langle |u_n|^{2m} \rangle, \tag{7}$$

while for odd $q=2m+1$ we suggest the following definition:

$$S_{2m+1}(k_n)=\mathrm{Im}\langle u_{n-1}u_n u_{n+1}|u_n|^{2(m-1)} \rangle \quad \text{(GOY)}. \tag{8}$$

The definition of the odd structure function differs from the usual definition $S_{2m+1}(k_n)=\langle |u_n|^{2m+1} \rangle$. Our choice, Eq. (8), is motivated by our reluctance to use the nonanalytic function $|u_n|$. We will see that our definition yields $\zeta_3=1$ as an exact result, similar to Kolmogorov's exact result for ζ_3 in three-dimensional fluid turbulence. It was shown by numerical simulations that the choice of parameters $\lambda=2$ and $(a,b,c)=(1,-0.5,-0.5)$ leads to scaling exponents ζ_q that are numerically close to those measured in experimental hydrodynamic turbulence.

B. Additional properties

The GOY model shares with Navier-Stokes turbulence an analog of the 4/5 law. Assuming stationarity and using the quadratic invariants introduced above, we can obtain two identities involving third-order correlations. Multiplying Eq. (1) by u_n^* we have, neglecting viscosity,

$$\frac{d}{dt}S_2(k_n)=2k_0\lambda^n\left(a\lambda S_3(k_{n+1})+bS_3(k_n)+\frac{c}{\lambda}S_3(k_{n-1})\right)+p_n, \tag{9}$$

where

$$p_n=2\,\mathrm{Re}\langle u_n^* f_n \rangle, \tag{10}$$

and obviously $p_n=0$ for $n>n_L$. In stationary conditions the rate of change of $S_2(k_n)$ vanishes, and we find

$$a\lambda S_3(k_{n+1})+bS_3(k_n)+\frac{c}{\lambda}S_3(k_{n-1})=0. \tag{11}$$

This equation has a solution in the inertial interval:

$$S_3(k_n)=\frac{1}{k_n}\left[A+B\left(\frac{c}{a}\right)^n\right]. \tag{12}$$

The unknown coefficients A and B can be found by its matching with the ''boundary conditions'' at small k_n. To do so we can follow the considerations of Pissarenko *et al.* [4] and sum up Eq. (9) on all the shells from $n=0$ to an arbitrary shell M, where M is in the inertial interval. Using the conservation laws (i.e., $a+b+c=0$) we derive

$$0=\frac{d}{dt}\sum_{n=0}^{M} S_2(k_n) =2k_M[a\lambda S_3(k_{M+1})+(b+a)S_3(k_M)]+\overline{\epsilon}, \tag{13}$$

$$0=\frac{d}{dt}\sum_{n=0}^{M} S_2(k_n)\left(\frac{a}{c}\right)^n =2k_M\left(\frac{a}{c}\right)^M[a\lambda S_3(k_{M+1})+(b+c)S_3(k_M)]+\overline{\delta}, \tag{14}$$

where the rate of dissipation $\overline{\epsilon}$ and the spurious mean $\overline{\delta}$ are defined as

$$\overline{\epsilon}=\sum_{n=0}^{n_L} p_n, \quad \overline{\delta}=\sum_{n=0}^{n_L} p_n\left(\frac{a}{c}\right)^n. \tag{15}$$

Substituting the solution (12) into Eqs. (13) and (14), one relates the values of A and B to those of the fluxes $\overline{\epsilon}$ and $\overline{\delta}$. Now Eq. (12) becomes

$$S_3(k_n)=\frac{1}{2k_n(a-c)}\left[-\overline{\epsilon}+\overline{\delta}\left(\frac{c}{a}\right)^n\right]. \tag{16}$$

There are four different types of functional dependence of $S_3(k_n)$ on k_n, determined by the ratio c/a, as illustrated at Fig. 1. For $c/a<0$, this function has period-two oscillations that are caused by the existence of a nonzero flux of the second integral of motion, which is not positively defined in this region. For $c/a>0$, the second integral is positively defined and the function is monotonic. For $|c/a|<1$, the role of the second flux becomes irrelevant in the limit $n\to\infty$. Consequently the deviation of $S_3(k_n)$ from the scale invariant behavior $S_3(k_n)\propto 1/k_n$ decreases as n increases, see panels (a) and (b) of Fig. 1. In contrast, in the case $|c/a|>1$ the role of the energy flux becomes irrelevant in the limit of $n\to\infty$. In this case the properties of the model are completely determined by the flux of the second integral, see panels (c) and (d) of Fig. 1. In the sequel we will focus on the region

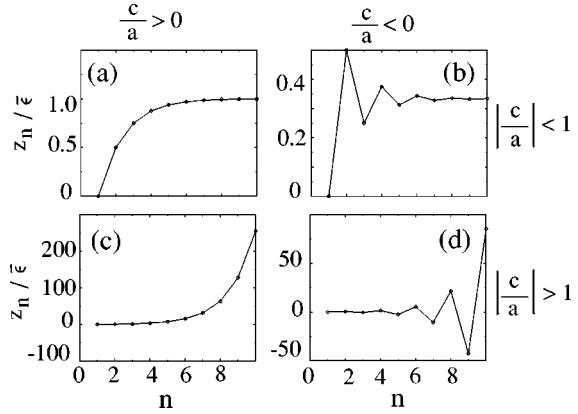

FIG. 1. Plots of the quantities $z_n=-k_nS_3(k_n)$ with $S_3(k_n)$ taken as the stationary solutions (16). The fluxes $\overline{\epsilon}$ and $\overline{\delta}$ are related by $\overline{\epsilon}=c\overline{\delta}/a$ and $a=1$. The four panels have different values of c. (a) $c=0.5$, (b) $c=-0.5$, (c) $c=2$, (d) $c=-2$.

$|c/a|<1$. The reason for this is that Navier-Stokes turbulence never exhibits a region in which the energy integral is irrelevant.

As we discussed, even in the ''physical'' region in which $|c/a|<1$, the subleading contributions (which are affected by the second integral) may influence the apparent scaling behavior of the leading scale invariant contributions, which are determined by the energy integral. In the region $-1<c/a<0$, which is commonly discussed in literature, subleading contributions lead to period-two oscillations that decrease upon the increase of n. These introduce additional problems in determining the scaling exponents. A simple way to eliminate this complication is to consider a ''helicity-free'' forcing chosen such that the flux of the second integral (''helicity'') would vanish identically. This is easilly achieved by selecting the forcing of the two first shells. From Eq. (15) we deduce

$$\overline{\delta}=0 \quad \text{at} \quad cp_0+ap_1=0, \quad p_2=p_3=\cdots=0. \tag{17}$$

For a random force that is Gaussian and δ-correlated in time,

$$\langle f_n(t)f_m(t')\rangle=\sigma_n^2\Delta_{nm}\delta(t-t'), \tag{18}$$

one gets

$$p_n=\sigma_n^2. \tag{19}$$

For this type of forcing the condition of zero ''helicity'' flux (17) is achieved by choosing the forcing to have the mean-square amplitudes

$$c\sigma_0^2+a\sigma_1^2=0. \tag{20}$$

Under this condition the period-two oscillations disappear.

The GOY model has some properties that make it undesirable for further analytic studies. It is best to exhibit these in comparison with the new (and we believe superior) model.

III. OUR MODEL: DEFINITION AND MAIN FEATURES

A. Our model

We propose the following equation of motion for our model:

$$\frac{du_n}{dt}=i(ak_{n+1}u_{n+2}u_{n+1}^*+bk_nu_{n+1}u_{n-1}^*-ck_{n-1}u_{n-1}u_{n-2}) - \nu k_n^2u_n+f_n, \tag{21}$$

where for simplicity we assume that the coefficients a, b, and c are real. As in the GOY model, conservation of energy in the inviscid limit is obtained if $a+b+c=0$.

The fundamental difference with the GOY model lies in the number of complex conjugation operators used in the nonlinear terms. We show in the following that this slight change is responsible for a difference in the phase symmetries of the two models. As a consequence, our model will exhibit shorter-ranged correlations than the GOY model. Apart from this difference, all the calculations described in the preceding section remain valid. Both models share the same quadratic invariants and one can derive for the our model another analog of the 4/5 law. We need to replace the definition of the odd order correlators (8) according to

$$S_3(k_n)=\mathrm{Im}\langle u_{n-1}u_nu_{n+1}^*\rangle,$$
$$S_{2m+1}(k_n)=\mathrm{Im}\langle u_{n-1}u_n|u_n|^{2(m-1)}u_{n+1}^*\rangle \quad \text{(Ours)}. \tag{22}$$

Note that the shell index n is related to the intermediate shell involved in the correlation function.

B. Phase symmetry and correlations

Let us examine the phase transformation:

$$u_n\rightarrow u_n\exp(i\theta_n). \tag{23}$$

The equations of motion of both the GOY and our models remain invariant under such transformations, provided that the phases θ_n are related by

$$\theta_{n-1}+\theta_n+\theta_{n+1}=0 \quad \text{(GOY)},$$
$$\theta_{n-1}+\theta_n-\theta_{n+1}=0 \quad \text{(Ours)}. \tag{24}$$

The phases θ_n can then be obtained iteratively from θ_1 and θ_2, namely

$$\theta_{1+3p}=\theta_1, \quad \theta_{3p+2}=\theta_2, \quad \theta_{3p}=-\theta_1-\theta_2 \quad \text{(GOY)}; \tag{25}$$

$$\theta_n=\frac{1}{\sqrt{5}}[\theta_1(\alpha_+^{n-2}-\alpha_-^{n-2})+\theta_2(\alpha_+^{n-1}-\alpha_-^{n-1})],$$
$$\alpha_\pm=\frac{1}{2}(1\pm\sqrt{5}) \quad \text{(Ours)}. \tag{26}$$

Although Eq. (26) has irrational numbers, it is easy to check that

$$\theta_n=r_n\theta_1+s_n\theta_2, \tag{27}$$

where r_n and s_n are integer numbers that grow exponentially with n.

Note that phases θ_1 and θ_2 satisfy the equations of motion

$$\frac{d\theta_1}{dt}=0, \quad \frac{d\theta_2}{dt}=0, \tag{28}$$

and they can be randomized by any small external forcing. It means that any correlation functions that contain the phases θ_1, θ_2 or both phases must be zero. In our direct numerical simulations, see below, we confirmed that this is indeed the case. In the our model there is only one nonzero second-order structure function. All nondiagonal correlation functions vanish in our model,

$$S_2(k_n,k_m)=\langle u_n u_m^*\rangle=0 \quad n\neq m \quad \text{(Ours)}. \tag{29}$$

This is not the case for the GOY model, for which there are correlations between shells separated by multiples of three:

$$S_2(k_n,k_{n+3p})\neq 0 \quad \text{(GOY)}. \tag{30}$$

The relative simplicity of our model is seen also with regards to higher-order structure functions. Our model has only one nonzero third-order structure function $S_3(k_n)$ that couples three consecutive shells as defined by Eq. (22). All other third-order structure functions vanish by averaging over the random phases θ_1 and θ_2. In contrast, in the GOY model there exists an infinite double set of nonvanishing correlation functions of third order with given n. These are

$$\langle u_n u_{n+3p} u_{n+1+3q}\rangle\neq 0 \quad \text{(GOY)}. \tag{31}$$

The same phenomenon occurs also for higher-order correlation functions. In the our model the number of nonzero correlation functions with finite n is much smaller than the corresponding functions in the GOY model, making it more convenient for theoretical analysis.

To conclude this section, we formulate a ''conservation law'' that determines which correlation functions of our model are nonzero. Introduce a quasimomentum κ_n for n shell by

$$\kappa_n \equiv \alpha^n, \tag{32}$$

where α is the golden mean, $\alpha^2=\alpha+1$. One can check that in our model the only nonzero correlation functions satisfy the following conservation law: *the sum of incoming quasimomenta (associated with u) is equal to the sum of outgoing quasimomenta (associated with u*).*

C. Additional properties

In this subsection we show that our model exhibits the properties of the GOY model that were revealed in Sec. II B.

With this aim we compute from Eq. (21) the time derivative of $S_2(k_n,t)$:

$$\begin{aligned}\frac{dS_2(k_n)}{dt}&=2\,\mathrm{Re}\left\langle \frac{du_n(t)}{dt}u_n^*(t)\right\rangle \\ &=-2\,\mathrm{Im}\,[ak_n\langle u_n^* u_{n+1}^* u_{n+2}\rangle+bk_n\langle u_{n-1}^* u_n^* u_{n+1}\rangle \\ &\quad -ck_{n-1}\langle u_{n-2}u_{n-1}u_n^*\rangle]-2\nu k_n^2\langle u_n u_n^*\rangle+p_n,\end{aligned} \tag{33}$$

where the forcing contribution p_n was defined in Eq. (10).

With the definition (22) of $S_3(k_n)$, this translates to the balance equation (9) derived for the GOY model. Note that these two models differ in the definitions of $S_3(k_n)$: Eq. (8) for the GOY model and Eq. (22) for our model. Clearly, $S_3(k_n)$ in our model has the same form (16) as in the GOY model and all the features of the GOY model discussed in Sec. II B are relevant for our model as well. In particular, one may eliminate the period-two oscillations by a proper choice (17) or (20) of the forcing.

The reader should note, however, that in the case of the GOY model the second- and the third-order structure functions have additional long-range correlations that do not appear in the balance equation. This is a flaw of the GOY model that is eliminated in the context of our model, where what you see is what exists. Note also that the long-range correlations for the GOY model exist between shells separated by multiples of three [see, for example, Eqs. (30) and (31)]. These correlations are responsible for period-three oscillations in scaling plots of the GOY model. These annoying oscillations are absent in our model by construction. Thus after elimination of the period-two oscillations (using ''helicity-free'' forcing) one finds scale invariant behavior of the structure functions almost from the very begining of the inertial interval.

IV. ASPECTS OF THE NUMERICAL INTEGRATION: STIFFNESS, FORCING, AND DISSIPATION

The numerical investigation of our model, as of any other stiff set of differential equations, calls for some care. We therefore dedicate this section to a discussion of the issues involved. A reader who wishes to consider the results only can skip this section and read the next one.

A. Stiffness

The main difficulty in integrating a shell model stems obviously from the stiffness of the system, i.e., we are concerned with a wide range of time scales in the system. Within the inertial range, the equation is dominated by the nonlinear terms so that the natural time scale (in the Kolmogorov approximation) of the nth shell scales as

$$\tau_n\sim\frac{1}{k_n u_n}\propto\frac{1}{k_n^{2/3}}. \tag{34}$$

Within the viscous range, however, the dominant term is the viscous one and if the nth shell lies in this subrange, its natural time becomes

$$\tau_n\sim\frac{1}{\nu k_n^2}. \tag{35}$$

We can now estimate the global stiffness of the system by quoting the ratio of the extremal time scales:

$$\frac{\tau_1}{\tau_N}\sim\frac{\tau_1}{\tau_{n_d}}\frac{\tau_{n_d}}{\tau_N}\sim\left(\frac{k_d}{k_1}\right)^{2/3}\left(\frac{k_N}{k_d}\right)^{2}\sim\lambda^{2[N+2(N-n_d)-1]/3}. \quad (36)$$

The global stiffness of the system thus depends both on the total number of shells N and on the width of the viscous region. Most of the results published in the literature are obtained with 22 shells, a forcing restricted to the first shell and a viscous boundary beginning about the 18th shell. In this typical case, we have $\tau_1/\tau_N\sim 6.6\times 10^5$. In this paper we typically use $N=34$ with about six shells in the viscous range. For this choice $\tau_1/\tau_N\sim 10^9$.

To deal with this stiffness we chose from the library SLATEC [7] the backward differentiation routine DDEBDF [8]. This routine is specially dedicated to very stiff problems. Although rather fast, its precision is not exceptional and it is rather sensitive to functions that are not sufficiently smooth. In cases of failure of the backward differentiation routine, the code switches automatically to a 4/5th order Runge-Kutta algorithm. Both routines adapt their step size to fulfill a prescribed precision requirement. The backward differentiation routine adapts in addition its order between 1 to 5.

B. Random forcing

We generate the random forcing to guarantee zero mean value of the velocity. We use a time correlated noise, with a correlation time chosen to be the natural time scale at the forcing shell: $\tau=1/(k_{n_L}u_{n_L})$. Denoting the forcing term f, in case of an exponential correlation, the evolution of f is ruled by the equation

$$\frac{d}{dt}f=-\frac{f}{\tau}+\eta, \quad (37)$$

where η is an uncorrelated noise. The presence of this new equation in the system could in principle make the integration more cumbersome. Fortunately, the system being stiff, the typical time step used in the integration is very small compared with the forcing time scale τ (six orders of magnitude in a typical calculation with 22 shells). This allows us to integrate f separately with a first-order scheme. In the code, the forcing is updated at each new call of the integrator. The Gaussian exponentially correlated random forcing is computed (after proper initialization) according to a first-order scheme proposed by Fox *et al.* [9]:

$$f(t+dt)=f(t)E+\sigma\sqrt{-2(1-E^2)\log_{10}(\alpha)}\exp(i2\pi\beta), \quad (38)$$

where $E=\exp(-dt/\tau)$, σ is the standard deviation of f, and α and β two random numbers between 0 and 1.

C. Dimensional analysis

For the purpose of our numerical fits we consider, following [10], the dissipative boundary n_d, where the dissipative term balances the nonlinear term. At this boundary $k_d u_{n_d}^2$ is of the order of $\nu k_d^2 u_{n_d}$. In the viscous range $n>n_d$ one can guess a generalized exponential form:

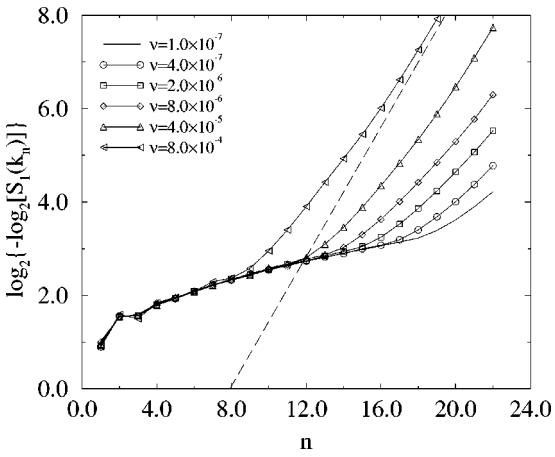

FIG. 2. Modulus of u_n in our model obtained by integration over 500 turnover time scales with values of the viscosities as shown in the figure. The dashed line represents the expected asymptotic behavior in the deep viscous regime. The slope of this line is given by Eq. (39).

$$u_n\sim k_n\exp\left[-\left(\frac{k_n}{k_d}\right)^x\right], \quad (39)$$

where [10]

$$x=\log_\lambda\frac{1+\sqrt{5}}{2}. \quad (40)$$

We have studied the influence of the width of the viscous range on this exponential behavior. The results obtained for a system of 22 shells with various viscosities are summarized in Fig. 2, where we can see that the scaling behavior in the viscous range approaches slowly the asymptotic prediction. In the case of the largest viscosity used, $\nu=8\times 10^{-4}$, we note that the asymptotic behavior starts at $n\simeq 15$ while $n_d\simeq 9$. We can then consider that this width of six shells is the minimal one needed to properly describe the viscous range.

In the inertial interval dimensional reasoning leads to K41 scaling: $u_n\sim(\overline{\epsilon}/k_n)^{1/3}$. This formula may be matched with Eq. (39):

$$u_n\sim u_{n_L}\left(\frac{k_{n_L}}{k_n}\right)^{1/3}\left[1+\left(\frac{k_n}{k_d}\right)^{4/3}\right]\exp\left[-\left(\frac{k_n}{k_d}\right)^x\right], \quad (41)$$

where $u_{n_L}\sim\sqrt{f/k_{n_L}}$ and $k_d\sim(f^3/\nu^6 k_{n_L})^{1/8}$. We will see that although the actual values of the exponents change due to multiscaling, the form of the solution is rather close to reality, and Eq. (41) is a good starting point for numerical fits.

V. NUMERICAL SIMULATIONS: RESULTS

A careful determination of the scaling exponents is a delicate issue. With an infinite inertial range, we expect pure scaling laws. Despite its large size, the inertial range that we have in shell models remains finite. The most widely used method to determine the exponent is based on a linear regression or on the determination of a local slope [11] in log-log scale. In these methods one needs a criterion to choose the fitting range. The uncertainty in the scaling expo-

nents comes obviously from the quality of the regression but also largely from the number of shells taken into consideration. We want to make the point here that these methods are not reliable, giving rise to a lot of confusion in the literature. One needs to fit a whole function to the inertial and dissipative ranges simultaneously to achieve reliable estimates of the exponents in the inertial range.

The definition of the scaling exponents can be a matter of choice of the statistical object. Our preferred definition is Eqs. (7) and (22) for even and odd exponents, respectively. Two alternative choices were widely used in the literature, respectively based on the modulus of the velocity and on the energy flux:

$$\tilde{S}_q(k_n) = \langle |u_n|^q \rangle, \tag{42}$$

$$\hat{S}_q(k_n) = \langle |\Sigma_n|^{q/3} \rangle = \langle |\mathrm{Im}[a\lambda\ u_n u_{n+1} u^*_{n+2} - c u_{n-1} u_n u^*_{n+1}]|^{q/3} \rangle. \tag{43}$$

The latter definition allowed for a higher numerical precision in the context of the GOY model because the energy flux is not affected either by the genuine dynamical oscillation (due to the helicity flux) or by the period-three oscillations. Beyond these different definitions of the statistical objects, we can also modify the definition of the scaling exponents themselves. In the framework of so-called ''extended self-similarity'' (ESS), instead of writing $S_q(k_n) = A k_n^{-\zeta_q}$ one assumes a scaling relation between the structure functions of order q and of order 3: $S_q(k_n) = A[S_3(k_n)]^{\tilde{\zeta}_q}$.

These different definitions give *a priori* different sets of scaling exponents. An efficient comparison, however, is difficult to set up in the case of the GOY model because of the various oscillations polluting the data. Moreover, none of the techniques described so far took explicitly into account the finite size effects. The fitting procedure that we describe now is an attempt to do so, and one of the results is that the exponents are universal, independent (for given parameters) of the choice of the statistical object.

In light of the interpolation formula (41), and encouraged by the fact that the dissipative, stretched exponential behavior is rather nicely obeyed, we fit all our spectra to the following fit formula:

$$F_q(k_n) = \frac{A_p}{k_n^{\zeta_q}} \left(1 + \alpha_q \frac{k_n}{k_{d,q}} \right)^{\mu_q} \exp\left[-\left(\frac{k_n}{k_{d,q}} \right)^x \right]. \tag{44}$$

This guarantees the right behavior at both asymptotics. Note that we do not make any hypothesis on the form of the transition between the power law and the dissipative regimes. In fitting we minimize the following error function:

$$\mathcal{E} = \sqrt{\sum_n \left(1 - \frac{\log_{10} F_q(k_n)}{\log_{10} S_q(k_n)} \right)^2}. \tag{45}$$

Here S_q refers to the numerically obtained structure function. We use the same fit formula for all three definitions of statistical objects. The sum in Eq. (45) was computed over the whole range except the two first shells and the two last shells in order to limit the effect of the boundaries. It turns out that the minimum found in this procedure is sharp (as a function of ζ_q) *provided* that we have a good fit of the S_q over its whole range. To estimate the relative error in the scaling exponents ζ_q we arbitrarily computed the values of ζ_q that agree with values of $\mathcal{E}$ that are twice the minimum value. These are the errors reported in all the tables below.

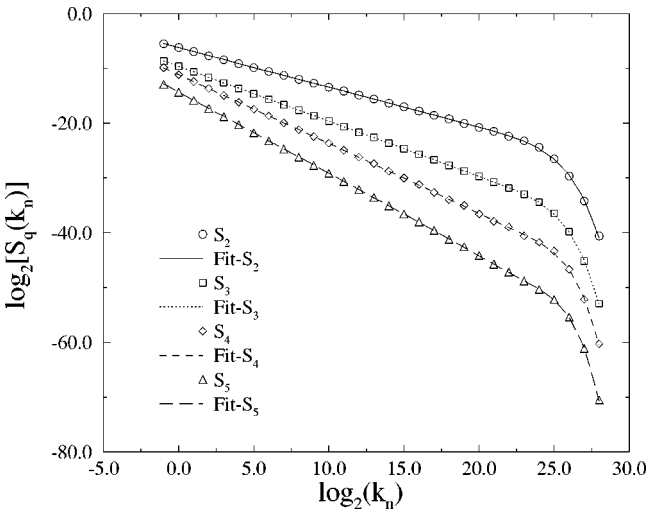

FIG. 3. Log-log plot of the structure functions $S_2(k_n)$ to $S_5(k_n)$ vs k_n and of the results obtained using the fitting formula (44). The structure functions are represented by the symbols and the fits by the lines.

In all our simulations we used the parameter values $a = 1$, $b = c = -0.5$, and $\sigma_1/\sigma_0 = 0.7$. This choice eliminates the flux of helicity and correspondingly the period-two oscillations in the scaling plots. Typical fits for the structure functions from S_2 to S_5 for simulations with 34 shells ($\nu = 4 \times 10^{-11}$, $\sigma_0 = 5 \times 10^{-3}$) are shown in Fig. 3.

In Table I we present the computed scaling exponents associated with three different definitions of q-order correlation functions. These results offer a very strong indication that the three scaling exponents of q-order correlation functions (with given q) are all the same.

On the other hand, we can make the point that ESS [12] in its standard usage does not seem be a useful approach in the present context for computing more accurate scaling exponents. In Fig. 4 we present $S_2(k_n)$ both as a function of k_n and as a function of $S_3(k_n)$. Even though superficially the ESS way of plotting seems to yield a longer linear plot, a careful examination shows a break in the inertial range scal-

TABLE I. Summary of the scaling exponents computed with a model of 34 shells.

q	S_q	$\langle \lvert u_n \rvert^q \rangle$	$\langle \lvert \Sigma_n \rvert^{q/3} \rangle$
1		0.393 ± 0.006	0.393 ± 0.007
2	0.720 ± 0.008	0.720 ± 0.008	0.719 ± 0.007
3	1.000 ± 0.005	1.003 ± 0.009	1.000 ± 0.005
4	1.256 ± 0.012	1.256 ± 0.012	1.249 ± 0.003
5	1.479 ± 0.006	1.488 ± 0.013	1.477 ± 0.004
6	1.706 ± 0.015	1.706 ± 0.015	1.691 ± 0.006
7	1.901 ± 0.010	1.910 ± 0.020	1.893 ± 0.010

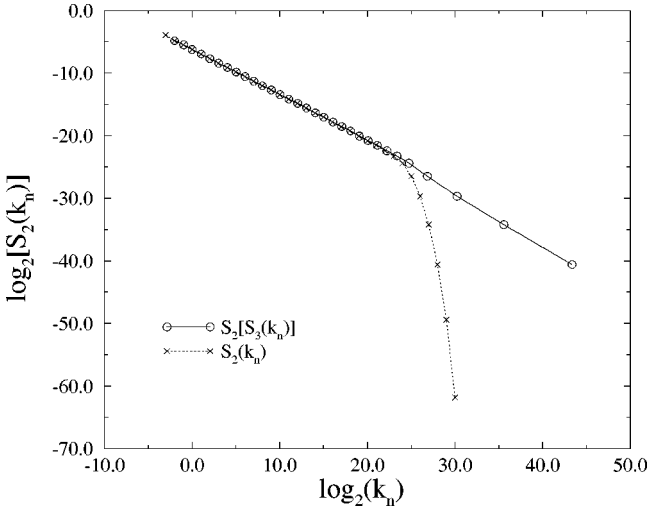

FIG. 4. Log-log plot of $S_2(k_n)$ vs k_n and vs $S_3(k_n)$, respectively. This plot shows that at least for this model, and when the accuracy is sufficiently high, ESS is quite useless in increasing the effective range of power-law behavior.

ing that occurs precisely at the crossover to dissipative behavior. We gain nothing from ESS for this model.

Nevertheless, for the limited aim of computing a precise value of ζ_2, we can make use of the ESS idea provided that we fit the whole range. To do this, we have to impose additional information on the fitting function. For the case of ζ_2 we can employ the information contained in the balance equation (9), closing it with the ansatz

$$S_2(k_n)=A_2|S_3(k_n)|^{\zeta_2}. \tag{46}$$

Using Eq. (46) and introducing $z_n=-k_nS_3(k_n)$, we can rewrite Eq. (9) as

$$z_{n+1}=z_{n-1}+b(z_{n-1}-z_n)-(k_n/k_*)^{2-\zeta_2}|z_n|^{\zeta_2}, \tag{47}$$

where $k_*=(\nu A_2)^{1/(\zeta_2-2)}$ and $a=1$.

Given z_0 and z_1, one can iteratively calculate z_n and, consequently, $S_3(k_n)$ and $S_2(k_n)$ in the range of k_n, for which the ESS ansatz is valid with reasonable accuracy. Assuming for simplicity $z_0=z_1$, the values of z_n are defined by three free parameters: z_0, A_2, ζ_2.

As an example, we applied this procedure to the numerical data calculated with $a=1$, $b=-0.5$, and $\nu=4\times10^{-11}$. The values of fitting parameters corresponding to the global minimum of the functional $\mathcal{E}$ (45) are $z_0=0.001\,26$, $A_2=1.80$, and $\zeta_2=0.728$. To estimate the accuracy of the chosen fit parameters, we have studied the dependence of $\mathcal{E}$ on the deviation $\delta\zeta_2$, δA_2, and δz_0 from their optimal values with two other parameters fixed at the optimal values. As before, we define the error bar for each parameter interval for which $\mathcal{E}$ takes on values that are twice the value at the minimum. With this definition $z_0=0.001\,26\pm0.000\,02$, $A_2=1.80\pm0.06$, and $\zeta_2=0.728\pm0.002$.

The accuracy reached here is higher than in the procedures described above. Most of the errors in the fit appear from the crossover region from power law to exponential decay. The analytically calculated $S_2(k_n)$ and $S_3(k_n)$ near the onset of the viscous range are very sensitive to the value of ζ_2. Therefore, employing an adequate fit in this region (which uses additional *a priori* information contained in the balance equation) allows one to be more accurate. Note that we do not have such simple balance equations for higher-order correlation functions and therefore a generalization of the procedure for higher orders is not available.

VI. TESTS OF THE STATISTICAL QUALITY OF THE NUMERICAL DATA

In evaluating the scaling exponents ζ_q one has to make sure that the structure functions $S_q(k_n)$ are calculated properly. This means that (i) the averaging time is sufficient for the representative statistics, and (ii) the numerical procedure produces an accurate realization $u_n(t)$.

A. The PDF test for the averaging time

In intermittent statistics one may need to wait a rather long time before the appearance of rare events that nevertheless contribute significantly to the statistics of q-order structure functions of n shells. This issue was carefully discussed by Leveque and She [13] in numerical simulations of the GOY model. They considered the waiting time Tn,q, which is needed to evaluate safely q-order correlations of n shells. They argued that times of the order of 5×10^9 turnover times of the n shell are required for $q\approx15$.

In the beginning of this subsection we estimate analytically the waiting time $T_{n,q}$, which is needed to observe, say, 100 events contributing to $S_{2q}(k_n)$. This is done using the probability $W_{n,q}$ to observe one rare event in which the value of the velocity u_n hits the range that contributes mostly to the statistics of $S_{2q}(k_n)$. Denoting by τ_n the decorrelation time on the nth shell we estimate

$$T_{n,q}\sim100\tau_n/W_{n,q}. \tag{48}$$

The probability $W_{n,q}$ may be related to the PDF of the velocity at the nth shell, $P_n(u)$. For the sake of this estimate we take $P_n(u)$ as a stretched exponential. We do not imply that this distribution function is realized in this model (in fact we know that it is not consistent with multiscaling). We use it only for the sake of an order of magnitude analytical estimate of the waiting time. Consider

$$P_n(v)=C\exp[-|v|^{\delta}], \tag{49}$$

where v is dimensionless velocity $v=u/u_0$, u_0 is a characteristic velocity, $u_0^2\simeq S_2(k_n)$, and C is a normalization constant. One computes $S_{2q}(k_n)$ as

$$S_{2q}(k_n)=u_0^{2q}\int_{-\infty}^{\infty}v^{2q}P_n(v)dv. \tag{50}$$

The integrand in Eq. (50) has a maximum at $v=v_q$, where

$$v_q=(2q/\delta)^{1/\delta}. \tag{51}$$

From Eq. (49) we can estimate the probability that v will attain a value within an interval of order of $\sqrt{q}\sim1$ around v_q, which was denoted as $W_{n,q}$. This interval of v values contributes maximally to S_{2q}. Namely,

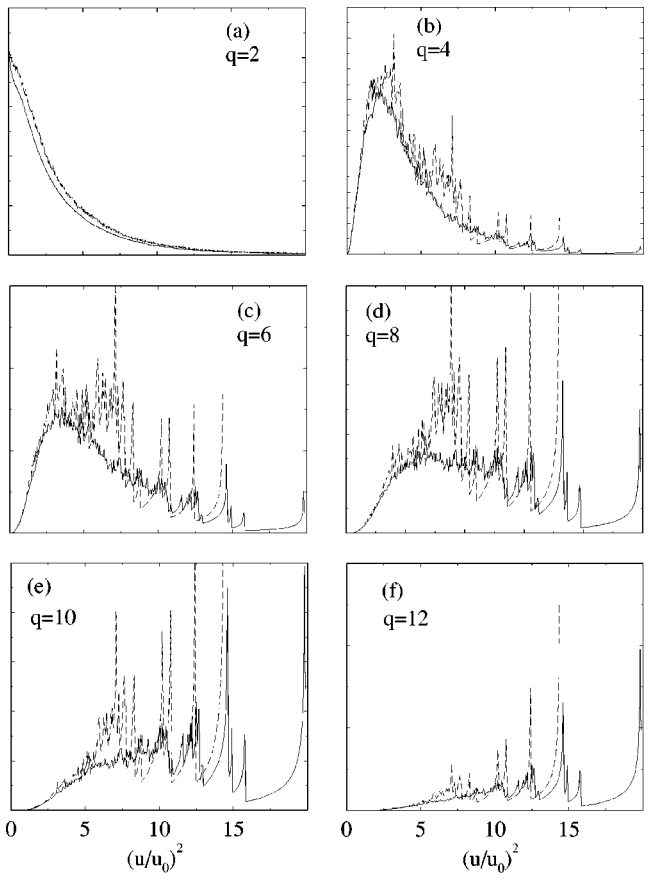

FIG. 5. Plots of $(u/u_0)^q P_3((u/u_0)^2)$ for the third shell with different values of q as shown in the figures. In every figure results are presented for 6250 (solid line) and 625 (dashed line) turnover times τ_3. Already S_8 is not accurate even with the longer run.

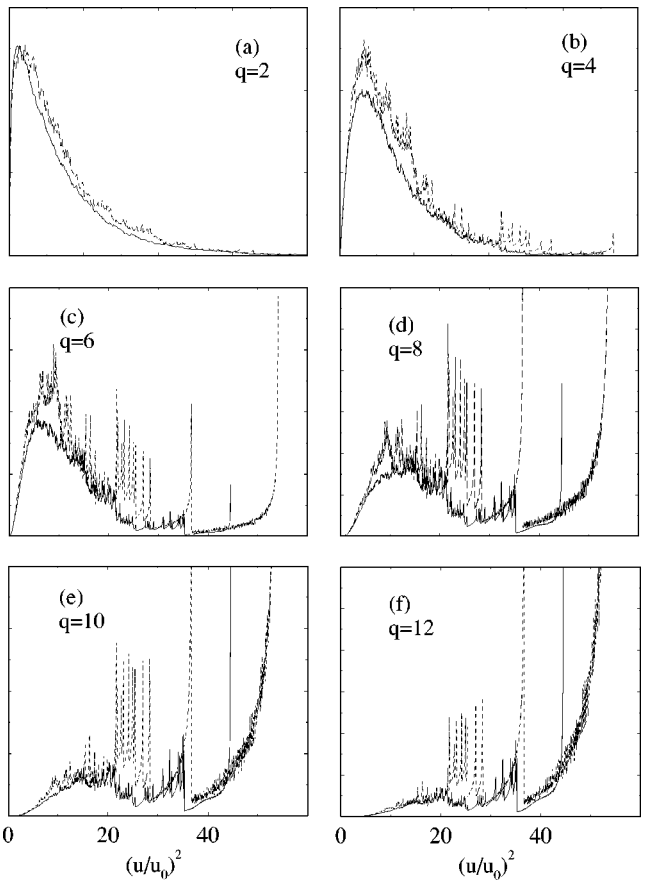

FIG. 6. Same as Fig. 5 but for shell no. 7. The solid line represents a longer run of $4\times10^4\tau_7$, and the dashed line a shorter run of $4000\tau_7$.

$$W_{n,q}\sim P_n(v_q)=C\exp[-2q/\delta]. \tag{52}$$

Equation (52) leads to the estimate

$$T_{n,q}\sim 100\tau_n\exp(2q/\delta), \tag{53}$$

where τ_n is a characteristic decorrelation time for n's shell. The time $T_{n,q}$ is exponentially large. For instance, for $\delta=1$ and $2q=10$, the averaging time required for accurate measurement of $S_{10}(k_n)$ is of the order of

$$T_{n,q}\simeq 100e^{10}\tau_n\simeq 2\times10^6\tau_n. \tag{54}$$

Admittedly this evaluation is rather rough. More accurate evaluations should be based on the numerically computed probability distribution functions as done for the GOY model in [13]. We plot the numerical value of $(u/u_0)^{2q}P(u^2/u_0^2)$ versus $(u/u_0)^2$ and see how noisy is the region that gives the main contribution to S_{2q}. Such plots for the third shell are presented at Fig. 5 for two realizations, one averaged over 625 and the other over 6250 turnover times of this shell, τ_3. In panels (a), (b), and (c) we show the integrands for S_2, S_4, and S_6. One sees that S_2 and S_4 can be evaluated reasonably well even from the shorter run, while S_6 can be computed only from the longer run. Panels (d), (e), and (f) present the analysis for S_8, S_{10}, and S_{12} correspondingly. The evaluation of S_8 is questionable even when the long run is used; the results for S_{10}, S_{12}, etc. are meaningless even for the run of 6250 turnover times. This run is too short for this purpose. The same analysis for shell no. 7 (in the bulk of the inertial interval), with two runs of $4000\tau_7$, shows that the improvement of the long run is not sufficient (see Fig. 6). We can hardly compute S_8 from the longer run. In the viscous end of the inertial interval (say for shell no. 12) our run was ten times longer ($4\times10^5\tau_{12}$) and the results can be seen in Fig. 7. Now S_8 can be computed reasonably well, but S_{10} is still buried in noise. Higher-order structure functions cannot be estimated at all. Lastly, in Fig. 8 we present results for shell no. 16, which belongs to the beginning of the viscous subrange. Here we have an even longer run of $2.5\times10^6\tau_{16}$, resulting in a marginal improvement in the ability to compute S_{10}.

For the evaluation of the scaling exponent ζ_q one needs to compute $S_q(k_n)$ throughout the inertial interval. It appears that we can determine scaling exponents up to ζ_6 from runs whose duration is about 5000 (longest) turnover times. In order to find exponents up to ζ_8 we need runs of minimal duration of 10^5 (longest) turnover times. An accurate determination of the exponent ζ_{10} calls for runs of about one million turnover times. Note that this estimate is in agreement with the simple analytical formula (54) presented above. Note also that these conclusions may very well be applicable also for the analysis of experimental data of hydrodynamic turbulence. The scaling exponents with our choice of parameters in our model correspond to those of Navier-Stokes turbulence, and it is likely that the far end of

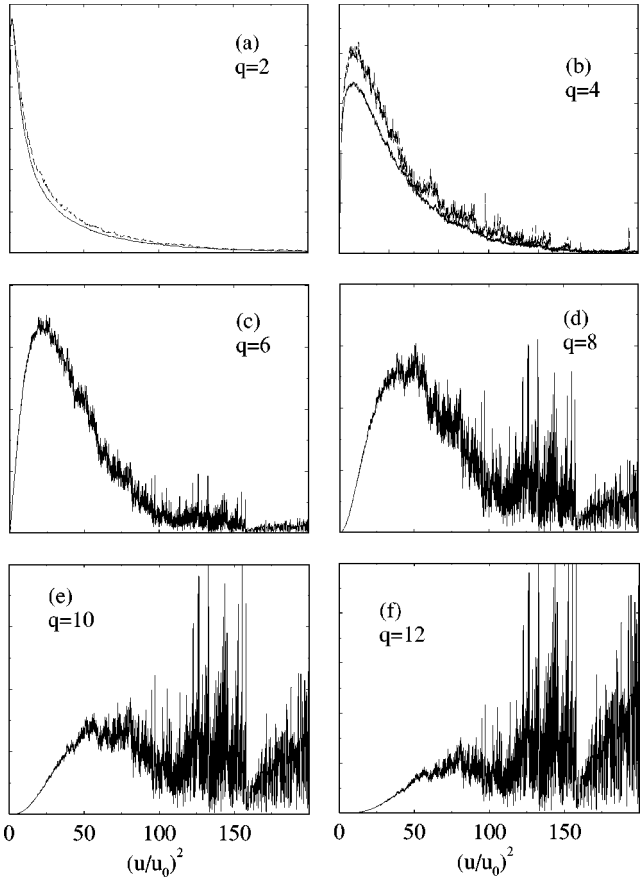

FIG. 7. Same as Fig. 5 but for shell no. 12. The solid line represents a longer run of $4\times10^5\tau_{12}$, and the dashed line a shorter run of $4\times10^4\tau_{12}$.

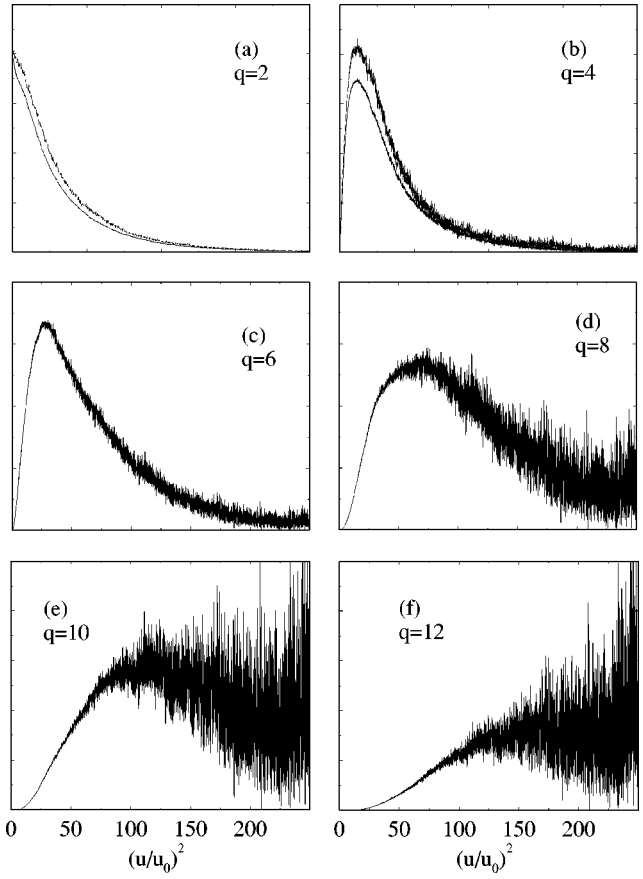

FIG. 8. Same as Fig. 5 but for shell no. 16. The solid line represents a longer run of $2.5\times10^6\tau_{16}$, and the dashed line a shorter run of $2.5\times10^5\tau_{16}$.

the probability distribution functions is as hard to reproduce in experiments as in our simulations. Since very long runs are rarely available in experimental data, this should serve as a warning that stated numerical values of higher scaling exponents should be taken with great caution.

B. Test of the numerical procedure

The averaging time is not the only factor affecting the quality of the numerical data. Since the time dependence of $u_n(t)$ is highly intermittent, we need to test carefully the ability of the numerics to cope with this. We need to check that the statistical characteristics of the process $u_n(t)$ obey the exact relations imposed on the correlation functions. A simple test can be built around the first equation of the infinite hierarchy relating $S_q(k_n)$ and $S_{q+1}(k_n)$. Consider Eq. (9) relating S_2 and S_3. In the inertial range, where the viscous term may be neglected, the largest term on the left-hand side (proportional to c) is balanced by the two first terms on the left-hand side. In the viscous range, where $S_3(k_n)$ drops to zero very quickly, this term is balanced by the viscous term on the right-hand side. It is thus useful to rewrite Eq. (9) in the form of a ''balance coefficient'' [keeping in mind that $S_3(k_n)$ is negative and $S_2(k_n)$ is positive]:

$$C(k_n)=\frac{a|S_3(k_{n+1})|k_{n+1}+b|S_3(k_n)|k_n-\nu k_n^2 S_2(k_n)}{c|S_3(k_{n-1})|k_{n-1}}. \tag{55}$$

If the numerical data satisfy the balance equation (9) accurately, the coefficients $C(k_n)$ have to be unity for all n. In Fig. 9 we show that in our simulations this relation between $S_3(k_n)$ and $S_2(k_n)$ is obeyed with accuracy better than 0.1%. However, this does not mean that less frequent events that contribute to higher-order correlation functions are also correctly reproduced. To check the statistical reliability of $S_4(k_n)$ one can use the second equation from the hierarchy, which connects $S_4(k_n)$ and $S_5(k_n)$ and so on. To measure this accuracy one can define, analogously to $C(k_n)$, a generalized balance coefficient $C_n^{(2q)}$. To define it we consider the time derivative of $S_{2q}(k_n)$:

$$\begin{aligned}\frac{dS_{2q}(k_n)}{dt}=&-2q\,\mathrm{Im}\,[ak_{n+1}\langle u_n^* u_{n+1}^* u_{n+2}|u_n|^{2(q-1)}\rangle\\&+bk_n\langle u_{n-1}^* u_n^* u_{n+1}|u_n|^{2(q-1)}\rangle\\&-ck_{n-1}\langle u_{n-2}u_{n-1}u_n^*|u_n|^{2(q-1)}\rangle]\\&-2q\nu k_n^2\langle|u_n|^{2q}\rangle.\end{aligned} \tag{56}$$

In the stationary case this gives

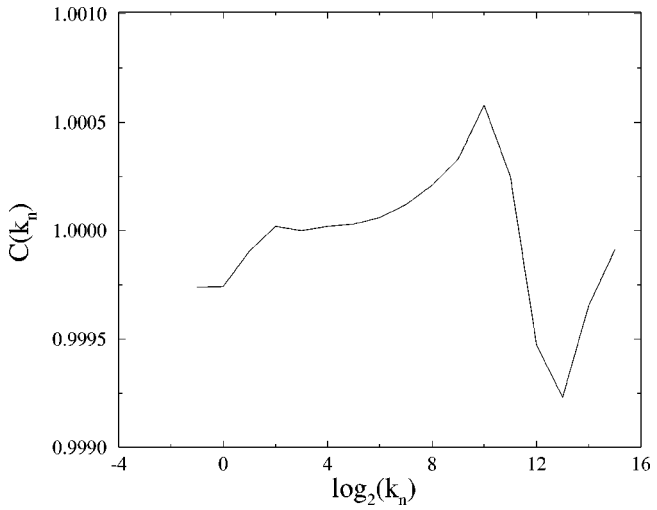

FIG. 9. Balance coefficient $C(k_n)$ for 22 shells, $b=-0.5$, average over 2500 largest turnover times.

$$aS^{-}_{2q+1}(k_{n+1})k_{n+1}+bS_{2q+1}(k_n)k_n+cS^{+}_{2q+1}(k_{n-1})k_{n-1} = \nu k_n^2 S_{2q}(k_n). \tag{57}$$

Here S_{2q+1} is defined by Eq. (22) and we have introduced two additional structure functions:

$$S^{\pm}_{2q+1}(k_n)=\mathrm{Im}\langle u_{n-1}u_n u^*_{n+1}|u_{n\pm1}|^{2(q-1)}\rangle. \tag{58}$$

One can rewrite Eq. (57), similarly to Eq. (55), in the form of a balance coefficient:

$$C_n^{(2q)}=\frac{aS^{-}_{2q+1}(k_{n+1})k_{n+1}+bS_{2q+1}(k_n)k_n+\nu k_n^2 S_{2q}(k_n)}{c|S^{+}_{2q+1}(k_{n-1})|k_{n-1}}. \tag{59}$$

Again, if the numerical data reproduce the balance equation (57), the coefficient $C_n^{(2q)}$ has to be unity for all n. Testing this fact should be an integral part of the numerical solution of this model and similar models in the future.

VII. UNIVERSALITY WITH RESPECT TO HYPERVISCOSITY

''Hyperviscosity'' in shell models amounts to changing the viscous term in Eq. (21) with a term νk_n^{2m} with $m>1$. The effect of hyperviscosity on shell models is a matter of controversy. It was originally argued by She and Leveque [11] that in the GOY model there was no universality of the scaling exponents, the value of the latter being strongly dependent on the dissipation mechanism. The same observation has been made by Ditlevsen [14]. If true, this observation would cast a doubt either on the relevance of shell models in turbulence studies or on one of the most widely accepted hypotheses in fluid turbulence: the universality of the exponents in the scaling range. Note, for example, that many direct simulations of 3D turbulence use hyperviscosity. On the other hand, Benzi *et al.* have showed [15] that in the case

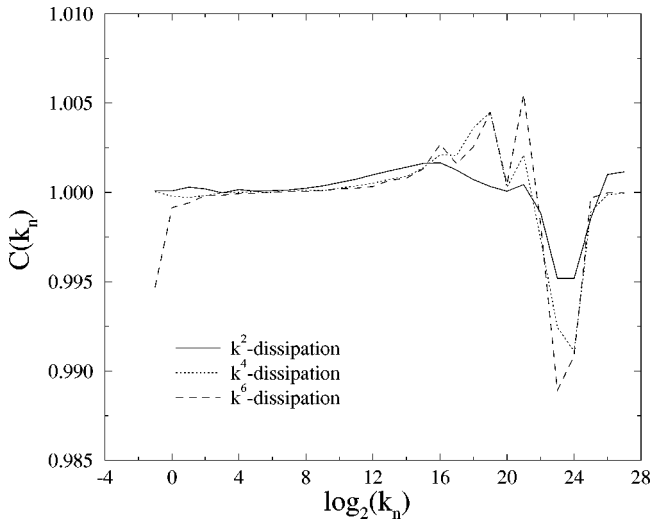

FIG. 10. Coefficients $C(k_n)$ [see Eq. (55)] obtained for a model of 34 shells integrated over 250 forcing turnover time scales with dissipative terms proportional to k_n^2, k_n^4, and k_n^6, respectively.

of shell models with eddy viscosity, the inertial exponents were independent of the particular definition used for the eddy viscosity. Recently we made the point [16] that within the GOY model this phenomenon is nothing but a finite size effect that disappears when one increases the size of the inertial range. We dedicate this section to showing that the same is true for the our model.

Before discussing the results, we need to test our simulations for accuracy of the evaluation of the structure functions. To this aim we present in Fig. 10 the balance coefficient $C_n^{(2)}$ (cf. Sec. VI B) for $m=1,2,3$. We tested the accuracy in a relatively short run of 250 forcing turnover time scales. The results indicate that even for this short run the accuracy of determination of the two lowest-order structure functions is about 0.1% in the inertial range, but only about 1% in the dissipative range. Note that hyperviscosity makes the determination of the structure functions in the viscous range (starting with the crossover region) somewhat less accurate. In order to reduce the source of uncertainty and without loss of generality, we measured the exponents from the flux-based structure functions (43).

In the following, we focus on the second- and third-order structure functions, using runs of duration 1500 forcing turnover time scales, and offer a careful calculation of their apparent scaling exponents as a function of the number of shells used in the simulations, and of the order of the hyperviscosity term m. We will show that the hyperviscous correction affects a finite number of shells in the vicinity of the viscous transition. This number is relatively large, about ten shells or three decades of ''length scales.'' The reason for this large effect is that we have a discrete model in which each shell interacts with four nearest neighbors. This means that with the standard shell spacing parameter $\lambda=2$, the local interactions spread over more than one decade of length scales. Nevertheless, we show now that this number remains unchanged when we increase the size of the inertial range, indicating a mere finite size effect.

To see this point examine Figs. 11 and 12, in which we superpose results for $k_n\Sigma_3(k_n)$ with $m=2$ and $m=3$, respec-

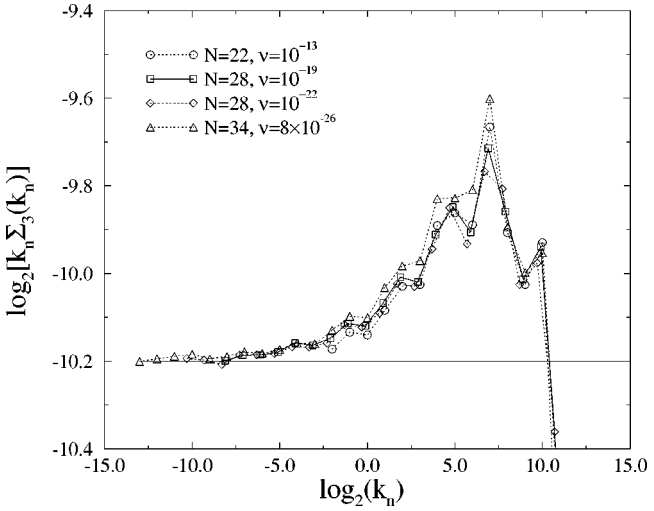

FIG. 11. Log-log plots of $k_n\Sigma_3(k_n)$ vs k_n in case of hyperviscosity of index $m=2$ with different numbers of shells and viscosities. The collapse has been obtained by shifting the abscissa. The solid line shows the constant behavior expected theoretically. One observes clearly that the departure from this constant value only occurs in a region of about ten shells near to the viscous transition. When the inertial range is large enough, the predicted behavior is recovered.

tively, which were obtained in eight different simulations as detailed in the figures. The plots are as a function of $\log_2(k_n)$ with an appropriate shift in the abscissa. We see that in all cases the region of deviation from a constant function, associated with the theoretical expectation Eq. (6), is of constant magnitude and of constant extent, independent of ν or the total number of shells. This is a clear indication that when the number of shells increases to infinity, the scaling exponent $\zeta_3=1$ will be observed in a universal manner.

Another way to reach the same conclusion is obtained by fitting structure functions as explained in Sec. VI to the formula (44). We ran simulations for $m=1$, 2, and 3 with $N=22$, 28, and 34. The exponent x of the viscous tail for $m=2,3$ exhibits significant departures from its dimensional expectation (40). We obtained $x\simeq 0.75$ for $m=2$ and $x\simeq 0.90$ for $m=3$, while $x\simeq 0.69$ for $m=1$. These values, which seem to be independent of the order of the structure function, have then been used in the fitting procedure. The results for ζ_2 and ζ_3 with normal viscosity were quite independent of N. On the contrary, hyperviscosity caused an apparent change in scaling exponents. However, as can be seen in Figs. 13 and 14, these values can be plotted as a function of $1/[\log_2(k_d/k_1)]^2$ and they converge, for $k_d\to\infty$ to the values obtained for $m=1$. Note that $\log_2(k_d/k_1)$ is precisely the length of the inertial interval, and k_d was obtained from the fit.

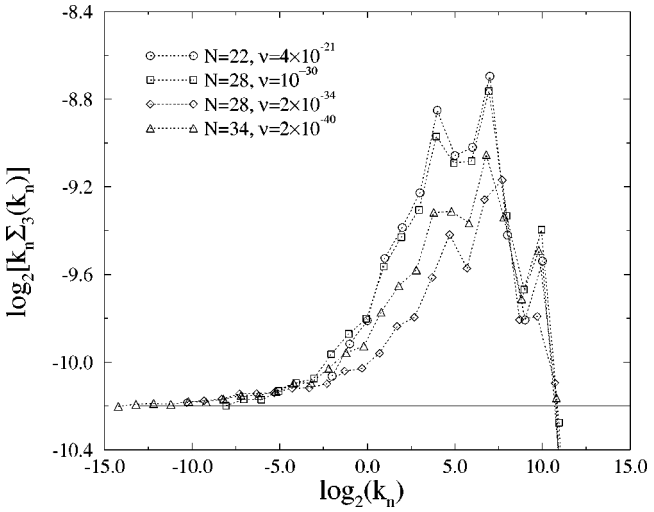

FIG. 12. Same as Fig. 11 in the case of hyperviscosity of index $m=3$. Note that the amplitude of the bump is larger than in the previous case.

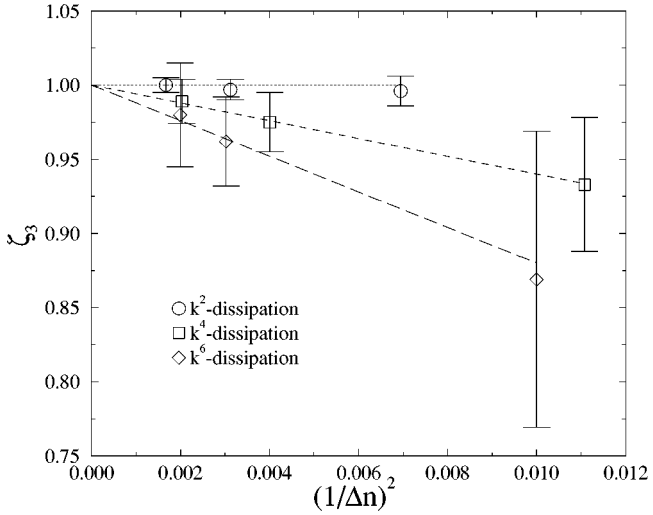

FIG. 13. Apparent scaling exponent ζ_3 as a function of the square of the inverse extent of the inertial interval, for $m=1$ (circles), $m=2$ (squares), and $m=3$ (diamonds). The tendency towards $\zeta_3=1$ is evident.

VIII. SUMMARY

We presented a shell model of turbulence, and demonstrated its improved properties in terms of simpler, shorter-

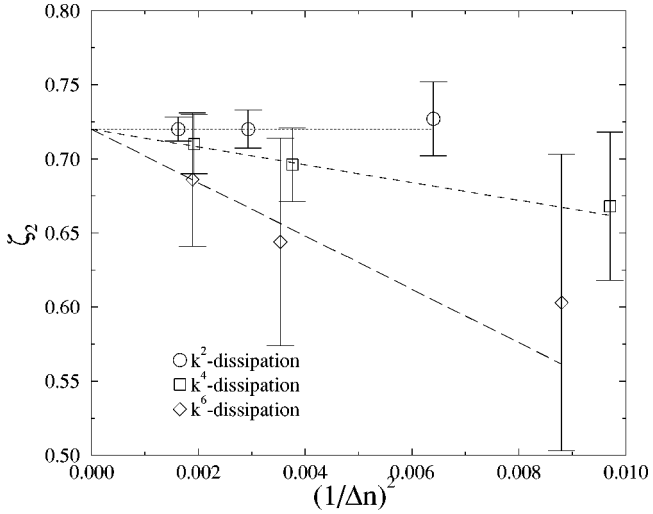

FIG. 14. Apparent scaling exponent ζ_2 as a function of the square of the inverse extent of the inertial interval, for $m=1$ (circles), $m=2$ (squares), and $m=3$ (diamonds). The tendency towards ζ_2 as found for normal viscosity $m=1$ is evident.

range correlations. The model exhibits anomalous scaling similar to the GOY model and to Navier-Stokes turbulence. In the future we will argue that the improved properties of this model help considerably in seeking analytic methods for the calculations of the scaling exponents. We used the opportunity of the introduction of this model to examine carefully issues such as the accuracy of determination of scaling exponents and the minimal length of running time required to achieve accurate structure functions. These considerations are model independent and pertinent to other examples of multiscaling as well. Lastly, we demonstrated the universality of the scaling exponents with respect to the type of viscous damping. This universality was questioned in the recent literature but we showed here for our model and previously [16] for the GOY model that there is no reason to doubt it.

ACKNOWLEDGMENTS

This work was supported in part by the U.S.–Israel Bi-National Science Foundation, The Basic Research Fund administered by the Israel Academy of Science and Humanities, The European Union under Contract No. FMRX-CT-96-0010, and the Naftali and Anna Backenroth-Bronicki Fund for Research in Chaos and Complexity.

[1] E. B. Gledzer, Dokl. Akad. Nauk SSSR **200**, 1043 (1973).
[2] M. Yamada and K. Ohkitani, J. Phys. Soc. Jpn. **56**, 4210 (1987).
[3] M. H. Jensen, G. Paladin, and A. Vulpiani, Phys. Rev. A **43**, 798 (1991).
[4] D. Pissarenko, L. Biferale, D. Courvoisier, U. Frisch, and M. Vergassola, Phys. Fluids A **5**, 2533 (1993).
[5] R. Benzi, L. Biferale, and G. Parisi, Physica D **65**, 163 (1993).
[6] V. I. Belinicher, V. S. L'vov, A. Pomyalov, and I. Procaccia, J. Stat. Phys. (to be published).
[7] SLATEC library (Sandia, Los Alamos, Air Force Weapons Laboratory Technical Exchange Committee), available on http://www.netlib.org/slatec
[8] L. F. Shampine and H. A. Watts, SAND-79-2374, DEPAC.
[9] R. F. Fox, I. R. Gatland, R. Roy, and G. Vemuri, Phys. Rev. A **38**, 5938 (1988).
[10] N. Schörghofer, L. Kadanoff, and D. Lohse, Physica D **88**, 44 (1995).
[11] E. Leveque and Z. S. She, Phys. Rev. Lett. **75**, 2690 (1995).
[12] R. Benzi, S. Ciliberto, R. Tripiccione, C. Baudet, F. Masaioli, and S. Succi, Phys. Rev. E **48**, R29 (1993).
[13] E. Leveque and Z. S. She, Phys. Rev. E **55**, 2789 (1997).
[14] P. Ditlevsen, Phys. Fluids **9**, 1482 (1997).
[15] R. Benzi, L. Biferale, S. Succi, and F. Toschi (unpublished).
[16] V. S. L'vov, I. Procaccia, and D. Vandembroucq, Phys. Rev. Lett. (to be published).